

Strong polaronic behavior in a weak coupling superconductor

Adrian G. Swartz^{1,2,3,*†}, Hisashi Inoue^{1,2,3,*}, Tyler A. Merz^{1,3}, Yasuyuki Hikita², Srinivas Raghu^{2,4}, Thomas P. Devereaux^{1,2}, Steven Johnston⁵, and Harold Y. Hwang^{1,2,3}

¹*Geballe Laboratory for Advanced Materials, Stanford University, Stanford, California 94305, USA*

²*Stanford Institute for Materials and Energy Sciences, SLAC National Accelerator Laboratory & Stanford University, Menlo Park, California 94025, USA*

³*Department of Applied Physics, Stanford University, Stanford, California 94305, USA*

⁴*Department of Physics, Stanford University, Stanford, California 94305, USA*

⁵*Department of Physics and Astronomy, University of Tennessee, Knoxville, Tennessee 37996, USA*

**These authors contributed equally to this work*

†Correspondence to: aswartz@stanford.edu

The origin of superconductivity in the dilute semiconductor SrTiO_3 has remained an open question for more than 50 years.^{1,2} The extremely low carrier densities (10^{17} - 10^{20} cm^{-3}) at which superconductivity occurs requires a commensurately large pairing potential. The majority of theoretical approaches consider electron-phonon (e-ph) coupling,^{3,4} and indeed there is experimental evidence for polarons – quasiparticles arising from strong e-ph coupling.^{5–9} Alternatively, more exotic scenarios involving plasmons or quantum critical ferro-

electric fluctuations have been proposed.¹⁰⁻¹² Using a newly developed method for engineering band alignments at oxide interfaces,^{13,14} we have measured the doping evolution of the dimensionless *e*-ph coupling strength (λ) and superconducting gap in Nb-doped SrTiO₃ by high resolution tunneling spectroscopy. In the normal state, we observe density of states (DOS) replicas at multiple phonon energies, indicating strong polaronic coupling ($\lambda \approx 1$) to the highest energy longitudinal optical (LO) phonon mode. Yet when cooled below the superconducting transition temperature T_c , we observe a single superconducting gap corresponding to the weak-coupling limit of Bardeen-Cooper-Schrieffer (BCS) theory,¹⁵ indicating an order of magnitude smaller coupling ($\lambda_{\text{BCS}} \approx 0.1$). This surprising result suggests the relevance of BCS beyond the Migdal limit in which it was derived, and that SrTiO₃ is an ideal system to probe superconductivity beyond the adiabatic condition.

Electron tunneling spectroscopy, which we employ here, has been instrumental in studying superconductivity mediated by *e*-ph coupling.¹⁶ The onset of superconductivity creates a gap (Δ) in the DOS near the Fermi energy (E_F), which can be resolved in high resolution tunneling experiments. In addition, for strong coupling, the *e*-ph interaction generates characteristic features in the differential conductance ($\sigma = di/dv$) as various phonon modes are traversed.¹⁷ In practice, energetically-defined tunneling into semiconducting SrTiO₃ has been extremely challenging due to the large dielectric constant ($\varepsilon \approx 20,000$ at low temperatures), which generates long depletion lengths (> 100 nm) and obscures direct tunneling processes. We overcome this problem using atomically engineered interface tunnel barriers,^{13,14} in which ultrathin epitaxial LaAlO₃(001) serves as a polar tunnel barrier in planar tunnel junctions (Fig. 1a,b). The LaAlO₃ provides an interfacial dipole, shifting the band alignments to

remove the depletion region (Fig. 1**c,d**).¹³ Using these dipole-tuned heterojunctions, we can newly access direct tunneling spectroscopy of bulk Nb-doped SrTiO₃ in *both* the normal and superconducting states, particularly at low electron densities.

Considering first the normal state, Fig. 1**e** shows a tunneling schematic of the enhanced conductance expected in the presence of *e*-ph coupling when biased at an optical phonon energy. Figure 1**f** shows experimental *di/dv* spectra in the positive bias regime (electron extraction from SrTiO₃) for several characteristic doping concentrations, with $E_F \approx 13$, 23, and 61 meV (see Supplementary Information¹⁸). Strikingly, we observe clear features of enhanced conductance at 40, 63, and 98 meV, arising from interactions with SrTiO₃ polar LO2, LO3, and LO4 modes, respectively.^{19,20} With doping, the spectroscopic lineshape evolves monotonically depending upon the ratio $E_F/\hbar\omega_{LO}$. In the dilute limit ($E_F < \hbar\omega_{LO}$), the crossing of the narrowly-occupied DOS with applied bias generates spikes in conductance, giving a spectroscopic measure of E_F and enabling resolution of the individual phonon contributions. In the other limit ($E_F \geq \hbar\omega_{LO}$), the DOS exhibits a continuum of additional tunneling states, leading to a step-like conductance enhancement. Thus, the lineshape of the enhanced conductance arising from *e*-ph coupling provides independent confirmation that the electronic structure probed at the interface reflects the intended bulk properties. Most importantly, we observe phonon interactions at energies above the top-most LO phonon branch ($eV > 0.1$ V) that appear at regular intervals of energy $\hbar\omega_{LO4}$, indicative of strong *e*-ph coupling.

The coupling of conduction electrons to polar optical phonons was first examined by Fröhlich,²¹ for which the *e*-ph interaction is given by

$$H_{e-\text{ph}} = \frac{1}{\sqrt{N}} \sum_{\sigma, \mathbf{k}, \mathbf{q}} M(\mathbf{q}) c_{\mathbf{k}+\mathbf{q}, \sigma}^\dagger c_{\mathbf{k}, \sigma} (b_{\mathbf{q}} + b_{-\mathbf{q}}^\dagger) \quad (1)$$

where $c_{\mathbf{k},\sigma}^\dagger$ and $b_{\mathbf{q}}^\dagger$ are the creation operators for an electron with wavevector \mathbf{k} and spin σ and phonon with wavevector \mathbf{q} , respectively. The interaction is highly momentum dependent with $M(\mathbf{q}) \propto 1/q$, resulting in a coupling strongly peaked at $q = 0$. To illucidate the impact that this type of coupling can have on the electronic bands and subsequent tunneling spectra, we first calculate the renormalized DOS (Fig. 2) for a single parabolic band coupled to an Einstein mode of $\hbar\omega = 100$ meV.¹⁸ The divergence at $q = 0$ is cut off by Thomas-Fermi screening with wavevector $q_{\text{TF}} = 0.1/a$ (a is the lattice constant) such that the matrix element is $M^2(q) = \frac{M_0^2}{q^2 + q_{\text{TF}}^2}$, where M_0 is adjust to set the value of λ . We note that $e\text{-ph}$ coupling peaked at $q = 0$ invalidates Migdal's theorem regardless of the value of the adiabatic ratio $E_F/\hbar\omega_{LO}$,²² therefore vertex corrections of order λ^2 generate non-negligible corrections to the self-energy. Nevertheless, since we are interested in a lower-bound estimate of the coupling, we proceed with Migdal-Eliashberg (ME) theory within the perturbative regime ($\lambda \leq 0.5$).^{22,23}

To estimate λ in SrTiO₃, we directly compare the relative intensities of the replicated DOS from ME theory with the experimental results, enabling a quantitative determination of the interactions without the need for model-dependent physical assumptions in the analysis of the data. Here direct measurements of d^2i/dv^2 are used, as shown in Fig. 3a, which provide higher sensitivity to multi-phonon processes.¹⁸ The measured peak positions indicate that the various LO modes are replicated at multiples of $\hbar\omega_{\text{LO4}}$ (see Fig. 3b), demonstrating strong coupling primarily to the LO4 branch. A relative increase in the spectral weight of multi-phonon processes is observed with decreasing carrier density (Fig. 3c). Figure 3d shows the measured intensity ratios, I_2/I_1 , for the LO4 mode together with the calculations of Fig. 2b. For the purposes of comparison, we extrapolate the ME predictions beyond the weak-coupling limit and plot the experimental I_2/I_1 along this line. Estimated in this way,

λ ranges from 0.6 and 1.4, where the highest doping concentration ($n = 1.6 \times 10^{20} \text{ cm}^{-3}$) exhibits replica amplitude ratios very close to the limit for which ME is viable.

The tunneling results presented thus far clearly indicate strong e -ph coupling in SrTiO₃ over a wide range of carrier densities, which is consistent with a growing body of experimental evidence for polaron formation. Our results are strikingly similar to recent photoemission observations of replica bands at the surface of SrTiO₃ arising from polaronic coupling to the LO₄ phonon, from which similar values of λ are deduced.^{8,9} These features have also been found in the novel 2D superconductors FeSe/SrTiO₃²⁴ and LaAlO₃/SrTiO₃,²⁵ as well as in anatase TiO₂.²⁶ A key aspect of Fröhlich e -ph coupling is the dominance of forward scattering, which is critical for generating replica bands with a curvature that mimics the main electronic band as seen experimentally, and yields dramatically different DOS modulations than q -linear coupling to acoustic modes.¹⁶ It is also consistent with magnetotransport, optical conductivity, and heat capacity experiments indicating large polaron formation in SrTiO₃.⁵⁻⁷ Thus despite the strong e -ph coupling present, mass renormalizations are relatively modest, and rather than self-trapped small polarons, highly mobile carriers are found even in the extremely dilute limit.²⁷ The question remains then: what is the relationship between the (strong) polaronic coupling and the pairing of electrons in the superconducting state?

Turning now to the superconducting state, we first note that within the simplest BCS expression,¹⁸ a naive estimate of T_c from our lower bound on λ would predict $T_c > 60$ K, in stark contrast to the observed $T_c \leq 0.4$ K. Spectroscopic examination of the superconducting phase can provide a direct measure of the pairing strength independent of the e -ph induced band renormalizations. Figure 4a shows a wide-scan di/dv spectrum measured below T_c for $n = 2.5 \times 10^{20} \text{ cm}^{-3}$ ($E_F \approx 70$ meV), corresponding to the overdoped side of the Nb:SrTiO₃

superconducting dome. Conductivity steps due to e -ph interactions are clearly evident, as well as the superconducting gap at low bias. A high-resolution scan (Fig. 4b) shows a single gap which is well fit by the BCS gap function, $\sigma_S/\sigma_N = \int_{-\infty}^{\infty} \nu(E) \frac{\partial f(E+eV)}{\partial E} dE$, where $f(E)$ is the Fermi function; $\nu(E) = \text{Re}[\frac{E-i\Gamma}{\sqrt{(E-i\Gamma)^2 - \Delta^2}}]$ is the BCS quasiparticle DOS, for which Γ is the quasiparticle broadening factor. Best fits to the data yield $\Delta = 42 \mu\text{eV}$ and $\Gamma = 2 \mu\text{eV}$. The $> 90\%$ suppression of the DOS in the superconducting gap and the low broadening indicates the very high quality of the junction, and places a lower bound on the quasiparticle lifetime, $\tau > 2 \text{ ns}$. Despite an early report of two superconducting gaps,²⁸ which motivated considerations of multiband superconductivity,²⁹ for all samples measured we have only observed a single gap, indicating that while at least two d -orbital bands are populated for these carrier densities, they are not spectroscopically distinct.

For conventional phonon-mediated superconductors, the strength of the pairing interaction can be determined by deviations from the universal thermodynamic relations of BCS theory. In particular, weak-coupling BCS predicts an exact ratio between the zero temperature gap ($\Delta(T = 0) \equiv \Delta_0$) and T_c of $2\Delta_0/k_B T_c = 3.53$, where k_B is Boltzmann's constant.¹⁵ In contrast, strong-coupling superconductors deviate from this value (i.e. Pb with $2\Delta_0/k_B T_c = 4.5$ and $\lambda = 1.3$), which is accounted for by including retardation corrections within ME.^{16,30} Due to the strong e -ph coupling observed in the normal state, we would expect SrTiO₃ to exhibit significant departures from weak-coupling BCS theory, particularly in the underdoped region where the largest values of λ are found. This, however, is not what we observe. Figure 4c plots $\Delta(T)$ (open circles, left axis) and the normalized resistivity ($\rho(T)/\rho_N$) (solid lines, right axis) for two characteristic samples corresponding to the overdoped and underdoped side of the Nb-doped superconducting dome. The temperature dependence is accurately described by $\Delta(T) = \Delta_0 \tanh[\frac{\pi}{1.76} \sqrt{\frac{2}{3} 1.43 (\frac{T_c}{T} - 1)}]$.³¹ Surprisingly,

we find $2\Delta_0/k_B T_c = 3.56 \pm .03$ and $3.59 \pm .05$ for the overdoped and underdoped samples, respectively, which is remarkably close to the weak-coupling limit, even compared with conventional superconductors.¹⁶ Using the BCS equation for T_c , we extract a coupling strength of $\lambda_{\text{BCS}} \approx 0.1$.¹⁸

Taken together, these experiments reveal an order of magnitude discrepancy between λ measured in the normal state versus λ_{BCS} , placing superconductivity in SrTiO₃ in a highly unusual regime (Fig. 4d). For conventional *e*-ph mediated superconductors, λ extracted from renormalizations to the band structure is in close quantitative correspondence to that needed to fully explain T_c within ME.^{16,17,30,32} For SrTiO₃, it may be inferred that the strong interaction with the LO4 mode is not effective in mediating pairing. This discrepancy could be assigned to the Coulomb potential, which would largely cancel the attractive interaction mediated by the LO4 phonon.³³ In the standard Coulomb pseudopotential (μ^*) approximation, this would require a large μ^* (> 0.5), far in excess of canonical values (< 0.25). Further, it should increase dramatically, commensurate with the variation in λ as the carrier density decreases. This, however, is inconsistent with the non-interacting behavior found in the dilute limit,^{27,34} where the highly polarisable lattice is very effective in dynamically screening the electrons.

Rather, an essential feature is the occurrence of superconductivity outside of the adiabatic approximation, which is a critical assumption underlying both BCS and its extension to strong-coupling in ME theory. Almost all of the superconducting dome in SrTiO₃ corresponds to an adiabatic (Migdal) ratio $\hbar\omega_{\text{LO4}}/E_{\text{F}} > 1$, and it is likely significant that a unity ratio corresponds to the loss of superconductivity in the overdoped regime. The nature of superconductivity outside of this so-called Migdal limit is poor due to the lack of reliable theoretical treatments. Yet in many high temperature superconductors, such as

the cuprates and pnictides, the bandwidth for quasiparticles is similar to the pairing energy scales related to either phonons or spin exchange, for example. In this context one may also consider SrTiO_3 to be a high temperature superconductor given the low carrier density, and our results offer a broader perspective of strong-coupling superconductivity beyond the adiabatic condition. Large coupling to high energy modes leads to strongly dressed quasiparticles with enhanced effective mass. However, this interaction does not lead to a comparable contribution to pairing, leaving acoustic phonons (or other low energy bosonic excitations) available to give rise to superconductivity out of these polarons, surprisingly well beyond the Migdal limit.

Methods

Nb-doped SrTiO_3 films were deposited on $\text{SrTiO}_3(001)$ substrates by pulsed laser deposition as described elsewhere.³⁵ Subsequently, 0 - 4 unit cells (u.c.) single crystal LaAlO_3 epitaxial layers were grown at $T = 650$ °C with $P = 1 \times 10^{-6}$ torr of O_2 with a fluence of 0.43 J/cm^2 . During growth, the LaAlO_3 thickness was monitored by reflection high-energy electron diffraction (RHEED) intensity oscillations. Except where indicated, 3 u.c. thick LaAlO_3 tunneling barriers were used throughout this study. The oxide heterostructure was then post annealed at $T = 400$ °C in 0.4 atm of O_2 for 45 min. Atomic force microscopy (AFM) measurements identified that the resulting surface was atomically flat over large areas ($> 50 \times 50 \mu\text{m}^2$) with step-and-terrace morphology. Nb-doped SrTiO_3 films grown in this regime exhibit bulk-like mobility values and full carrier activation.³⁵ The samples were transferred *ex situ* to an adjacent chamber for the deposition of metallic electrodes at room temperature through a shadow mask. Just prior to deposition, the films were pre-annealed at 500 °C in 1×10^{-5} torr of O_2 to remove adsorbates.¹⁴ For the superconducting gap measurements, we

employed Ag electrodes contacted by Au wire and Ag paint. Ohmic contacts were made to the Nb-doped SrTiO₃ film by wire bonding with Al wire. Details regarding the electronic measurements, fitting procedure, and DOS calculations are provided in the Supplemental Information.¹⁸

Acknowledgements

We acknowledge S. A. Kievelson, P. A. Lee, P. B. Littlewood, A. V. Maharaj, A. J. Millis, L. Rademaker, Z.-X. Shen, and Y. Wang for useful discussions. This work was supported by the Department of Energy, Office of Basic Energy Sciences, Division of Materials Sciences and Engineering, under Contract No. DE-AC02-76SF00515; FAME, one of six centers of STARnet, a Semiconductor Research Corporation program sponsored by MARCO and DARPA; and the Gordon and Betty Moore Foundation's EPiQS Initiative through Grant GBMF4415. S. J. acknowledges support from the University of Tennessee's Science Alliance Joint Directed Research and Development program, a collaboration with Oak Ridge National Laboratory.

Author Contributions

AGS and HI prepared the samples, performed the experiments, and analyzed the tunneling data. SJ developed and performed the theoretical calculations. TAM and YH assisted with measurements and sample growth. SJ, TPD, and SR provided theoretical insight and analysis. AGS, HI, and HYH conceived and designed the experiment. All authors contributed to the discussion and writing of the manuscript.

REFERENCES

¹Schooley, J. F., Hosler, W. R. & Cohen, M. L. Superconductivity in semiconducting SrTiO_3 . *Phys. Rev. Lett.* **12**, 474 (1964).

²Koonce, C. S., Cohen, M. L., Schooley, J. F., Hosler, W. R. & Pfeiffer, E. R. Superconducting transition temperatures of semiconducting SrTiO_3 . *Phys. Rev.* **163**, 380 (1967).

³Appel, J. Soft mode superconductivity in SrTiO_{3-x} and $\text{Ca}_y\text{Sr}_{1-y}\text{TiO}_{3-x}$. *Physica* **55**, 577 (1971).

⁴Gor'kov, L. P. Phonon mechanism in the most dilute superconductor n -type SrTiO_3 . *Proc. Natl. Acad. Sci.* **113**, 4646 (2016).

⁵Ahrens, M., Merkle, R., Rahmati, B. & Maier, J. Effective masses of electrons in n -type SrTiO_3 determined from low-temperature specific heat capacities. *Physica B: Condensed Matter* **393**, 239 (2007).

⁶Devreese, J. T., Klimin, S. N., van Mechelen, J. L. M. & van der Marel, D. Many-body large polaron optical conductivity in $\text{SrTi}_{1-x}\text{Nb}_x\text{O}_3$. *Phys. Rev. B* **81**, 125119 (2010).

⁷van der Marel, D., van Mechelen, J. L. M. & Mazin, I. I. Common fermi-liquid origin of T^2 resistivity and superconductivity in n -type SrTiO_3 . *Phys. Rev. B* **84**, 205111 (2011).

⁸Chen, C., Avila, J., Frantzeskakis, E., Levy, A. & Asensio, M. C. Observation of a two-dimensional liquid of Fröhlich polarons at the bare SrTiO_3 surface. *Nature Commun.* **6**, 9585 (2015).

⁹Wang, Z. *et al.* Tailoring the nature and strength of electron-phonon interactions in the $\text{SrTiO}_3(001)$ two-dimensional electron liquid. *Nature Mater.* doi:10.1038/nmat4623 (2016).

¹⁰Takada, Y. Theory of superconductivity in polar semiconductors and its application to n -type semiconducting SrTiO_3 . *J. Phys. Soc. Jpn.* **49**, 1267 (1980).

¹¹Ruhman, J. & Lee, P. A. Superconductivity at very low density: the case of strontium titanate. *arXiv preprint arXiv:1605.01737* (2016).

¹²Edge, J. M., Kedem, Y., Aschauer, U., Spaldin, N. A. & Balatsky, A. V. Quantum critical origin of the superconducting dome in SrTiO_3 . *Phys. Rev. Lett.* **115**, 247002 (2015).

¹³Yajima, T. *et al.* Enhanced electrical transparency by ultrathin LaAlO_3 insertion at oxide metal/semiconductor heterointerfaces. *Nano Letters* **15**, 1622 (2015).

¹⁴Inoue, H. *et al.* Origin of the magnetoresistance in oxide tunnel junctions determined through electric polarization control of the interface. *Phys. Rev. X* **5**, 041023 (2015).

¹⁵Bardeen, J., Cooper, L. N. & Schrieffer, J. R. Theory of superconductivity. *Phys. Rev.* **108**, 1175 (1957).

¹⁶Carbotte, J. P. Properties of boson-exchange superconductors. *Rev. Mod. Phys.* **62**, 1027 (1990).

¹⁷McMillan, W. L. & Rowell, J. M. Lead phonon spectrum calculated from superconducting density of states. *Phys. Rev. Lett.* **14**, 108 (1965).

¹⁸See supplementary information.

¹⁹Choudhury, N., Walter, E. J., Kolesnikov, A. I. & Loong, C.-K. Large phonon band gap in SrTiO_3 and the vibrational signatures of ferroelectricity in ATiO_3 perovskites: First-principles lattice dynamics and inelastic neutron scattering. *Phys. Rev. B* **77**, 134111 (2008).

²⁰Sroubek, Z. Electron tunneling in Indium- SrTiO_3 :Nb Schottky barriers. *Solid State Commun.* **7**, 1561 (1969).

²¹Fröhlich, H. Electrons in lattice fields. *Adv. Phys.* **3**, 325 (1954).

²²Wang, Y., Nakatsukasa, K., Rademaker, L., Berlijn, T. & Johnston, S. Aspects of electron-phonon interactions with strong forward scattering in FeSe thin films on SrTiO_3 substrates.

Supercond. Sci. Technol. **29**, 054009 (2016).

²³Grimaldi, C., Pietronero, L. & Strässler, S. Nonadiabatic superconductivity. II. Generalized Eliashberg equations beyond Migdal's theorem. *Phys. Rev. B* **52**, 10530 (1995).

²⁴Lee, J. J. *et al.* Interfacial mode coupling as the origin of the enhancement of T_c in FeSe films on SrTiO₃. *Nature* **515**, 245 (2014).

²⁵Cancellieri, C. *et al.* Polaronic metal state at the LaAlO₃/SrTiO₃ interface. *Nature Commun.* **7**, 10386 (2016).

²⁶Moser, S. *et al.* Tunable polaronic conduction in Anatase TiO₂. *Phys. Rev. Lett.* **110**, 196403 (2013).

²⁷Kozuka, Y., Susaki, T. & Hwang, H. Vanishing Hall coefficient in the extreme quantum limit in photocarrier-doped SrTiO₃. *Phys. Rev. Lett.* **101**, 096601 (2008).

²⁸Binnig, G., Baratoff, A., Hoenig, H. & Bednorz, J. Two-band superconductivity in Nb-doped SrTiO₃. *Phys. Rev. Lett.* **45**, 1352 (1980).

²⁹Fernandes, R. M., Haraldsen, J. T., Wölfle, P. & Balatsky, A. V. Two-band superconductivity in doped SrTiO₃ films and interfaces. *Phys. Rev. B* **87**, 014510 (2013).

³⁰Schackert, M. *et al.* Local measurement of the Eliashberg function of Pb islands: enhancement of electron-phonon coupling by quantum well states. *Phys. Rev. Lett.* **114**, 047002 (2015).

³¹Devereaux, T. P. & Einzel, D. Electronic Raman scattering in superconductors as a probe of anisotropic electron pairing. *Phys. Rev. B* **51**, 16336 (1995).

³²Allen, P. B. Empirical electron-phonon λ values from resistivity of cubic metallic elements. *Phys. Rev. B* **36**, 2920 (1987).

³³Morel, P. & Anderson, P. Calculation of the superconducting state parameters with retarded electron-phonon interaction. *Phys. Rev.* **125**, 1263 (1962).

³⁴Lin, X., Fauqué, B. & Behnia, K. Scalable T^2 resistivity in a small single-component Fermi surface. *Science* **349**, 945 (2015).

³⁵Kozuka, Y., Hikita, Y., Bell, C. & Hwang, H. Y. Dramatic mobility enhancements in doped SrTiO_3 thin films by defect management. *Appl. Phys. Lett.* **97**, 012107 (2010).

Figure 1. Dipole controlled interfaces for high resolution tunneling spectroscopy of Nb:SrTiO₃. Schematic diagrams of the tunneling junction depicting: **a**, the atomic layer stacking with interfacial LaAlO₃ dipole layer which serves as the tunneling barrier; **b**, device measurement geometry; **c-d**, resulting band diagrams without and with the insertion of the interface dipole; and **e**, enhanced conductance expected in the presence of e-ph coupling when biased at an optical phonon energy. **f**, Experimental normal state di/dv spectra for three characteristic doping concentrations measured at $T = 2$ K.

Figure 2. Renormalization of the electron band structure due to the Fröhlich interaction. **a**, Calculated spectral function for a single parabolic band ($E_F = 40$ meV and $m^* = 1.4m_0$, where m^* is the effective mass and m_0 is the bare electron mass), coupled to a single dispersionless phonon mode. The momentum dependence of the Fröhlich interaction generates replicas of the main electronic band, which are offset from the main band by multiples of the phonon energy. **b**, The momentum integrated DOS given by $-\sum_{\vec{k}} \text{Im}G(\vec{k}, \omega)/\pi$ for several values of λ , where $G(\vec{k}, \omega)$ is the dressed Green's function. Further details are provided in the Supplementary Information.

Figure 3. Doping dependence of the electron-phonon coupling in Nb:SrTiO₃. **a**, Second harmonic d^2i/dv^2 spectra for $n = 1.6 \times 10^{19}$ cm⁻³ measured at $T = 2$ K (black line, top panel). The contribution from interactions with the LO phonon modes are fit with the derivative of an asymmetric Lorentzian (red line, top panel) for which the integrated e-ph contribution to di/dv is shown in the bottom panel (grey curve). **b**, Extracted peak positions for the LO3 and LO4 phonon modes indicating that both modes are repeated at intervals of the LO4 energy, $\hbar\omega_{\text{LO4}} = 98$ meV. **c**, Amplitude of the phonon contribution

(LO4 only) as a function of bias for three different doping concentrations. **d**, Black squares show the intensity ratios for one phonon (I_1) and two phonon (I_2) processes calculated from the renormalized DOS (Fig. 2b). Measured data from **c** are plotted on the extrapolated black dashed line to obtain λ .

Figure 4. Superconducting tunneling spectroscopy of Nb-doped SrTiO₃.

a, Wide scan di/dv measured at $T = 40$ mK showing the interaction with the high energy phonon modes, as well as the superconducting gap at low bias (near $V = 0$ V). **b**, High resolution measurements of the superconducting gap for several temperatures. Dashed curve is the best fit for the 40 mK data to the BCS gap equation. For **a** and **b**, $n = 2.5 \times 10^{20}$ cm⁻³, corresponding with the overdoped side of the Nb:SrTiO₃ superconducting dome. **c**, Temperature dependence of the superconducting gap (Δ) (left axis) and resistivity (ρ) (right axis), normalized to the normal state value (ρ_N) measured at $T = 400$ mK. Overdoped: $n = 2.5 \times 10^{20}$ cm⁻³ (black data), underdoped: $n = 3.0 \times 10^{19}$ cm⁻³ (blue data). **d**, Comparison of the electron-phonon coupling (λ) with that extracted from the superconducting gap (λ_{BCS}) for Nb:SrTiO₃. This unconventional regime is evident when compared with conventional superconductors over a broad range of *e*-ph coupling (data compiled from Refs. 16, 17, 30, and 32).

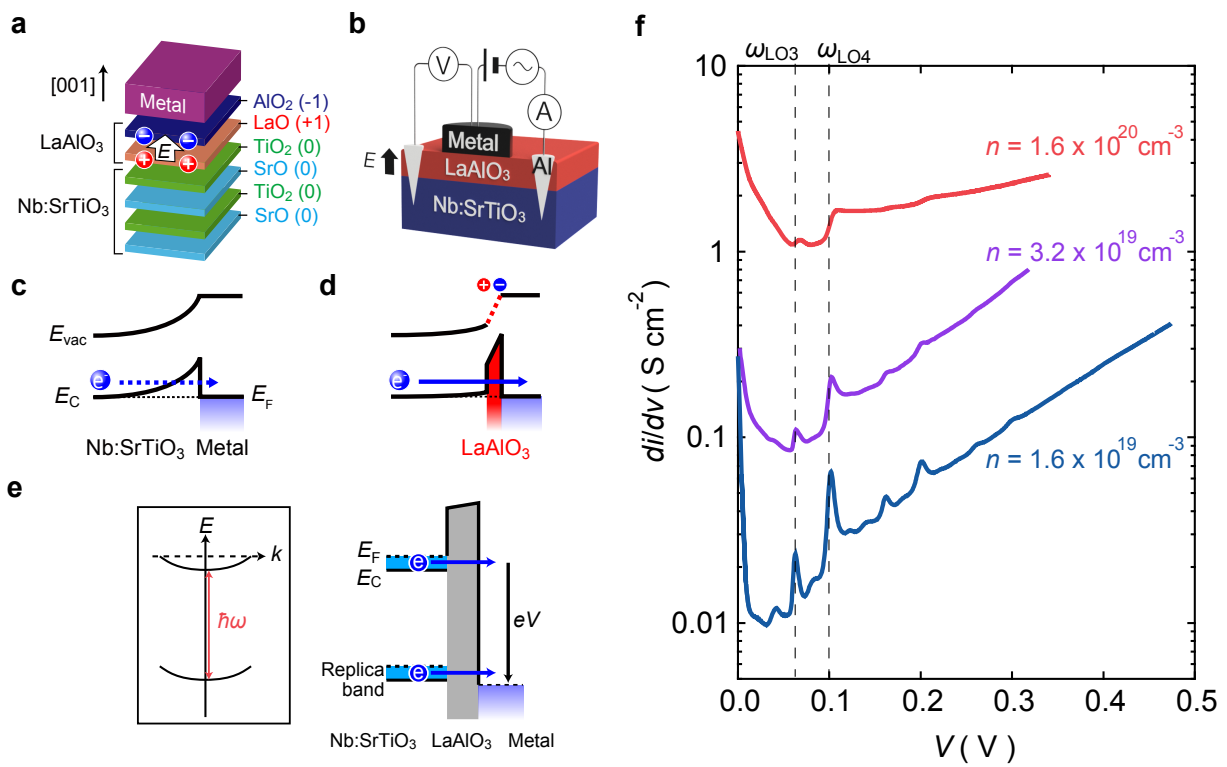


Figure 1.

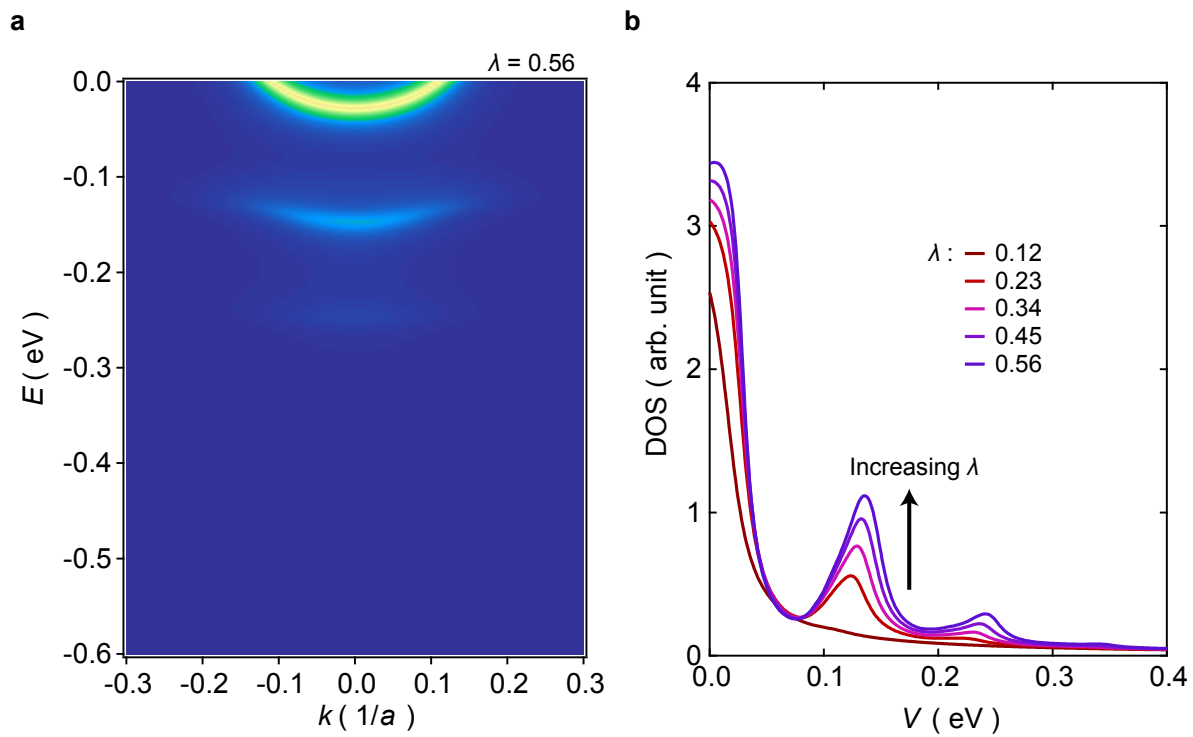


Figure 2.

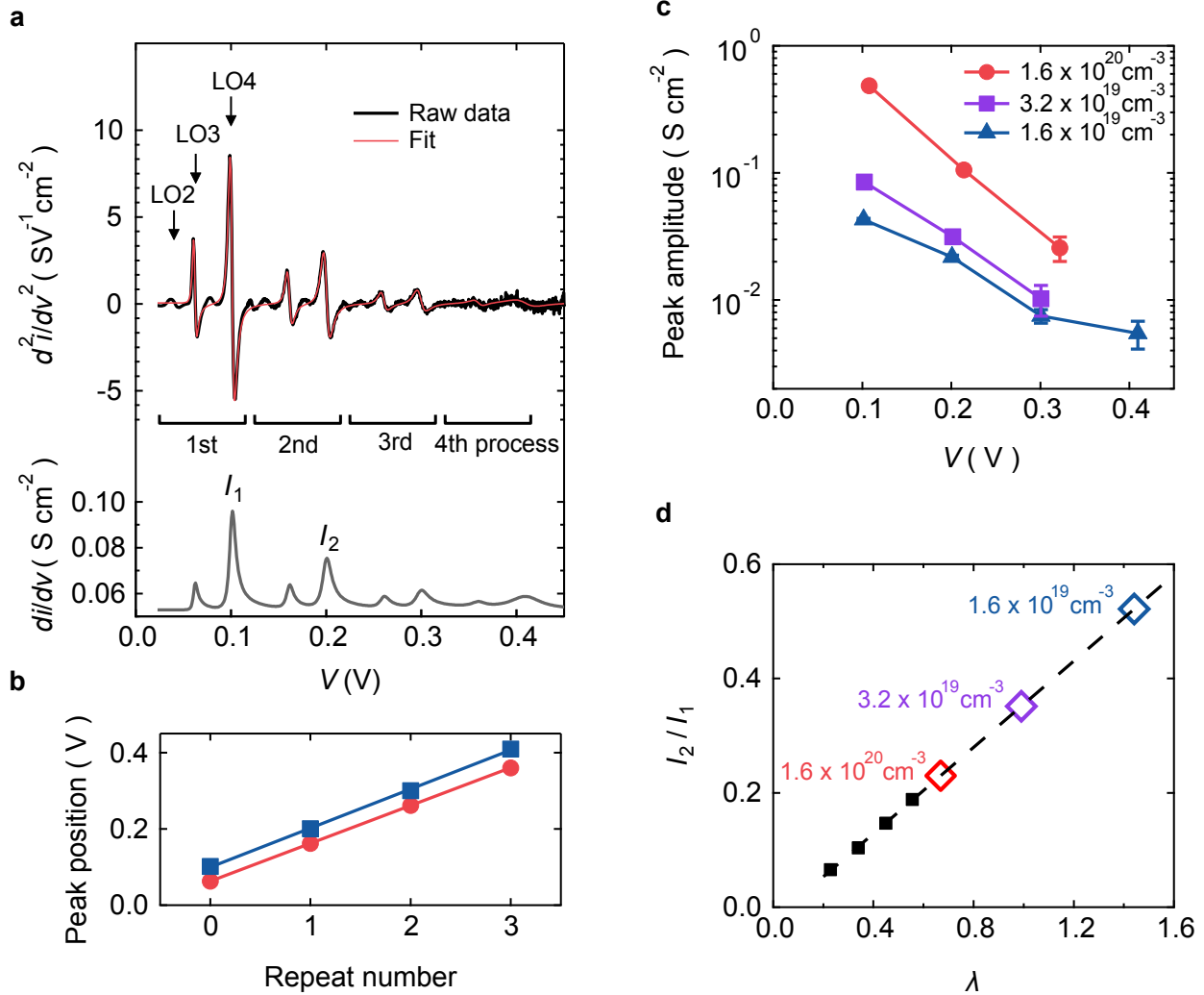


Figure 3.

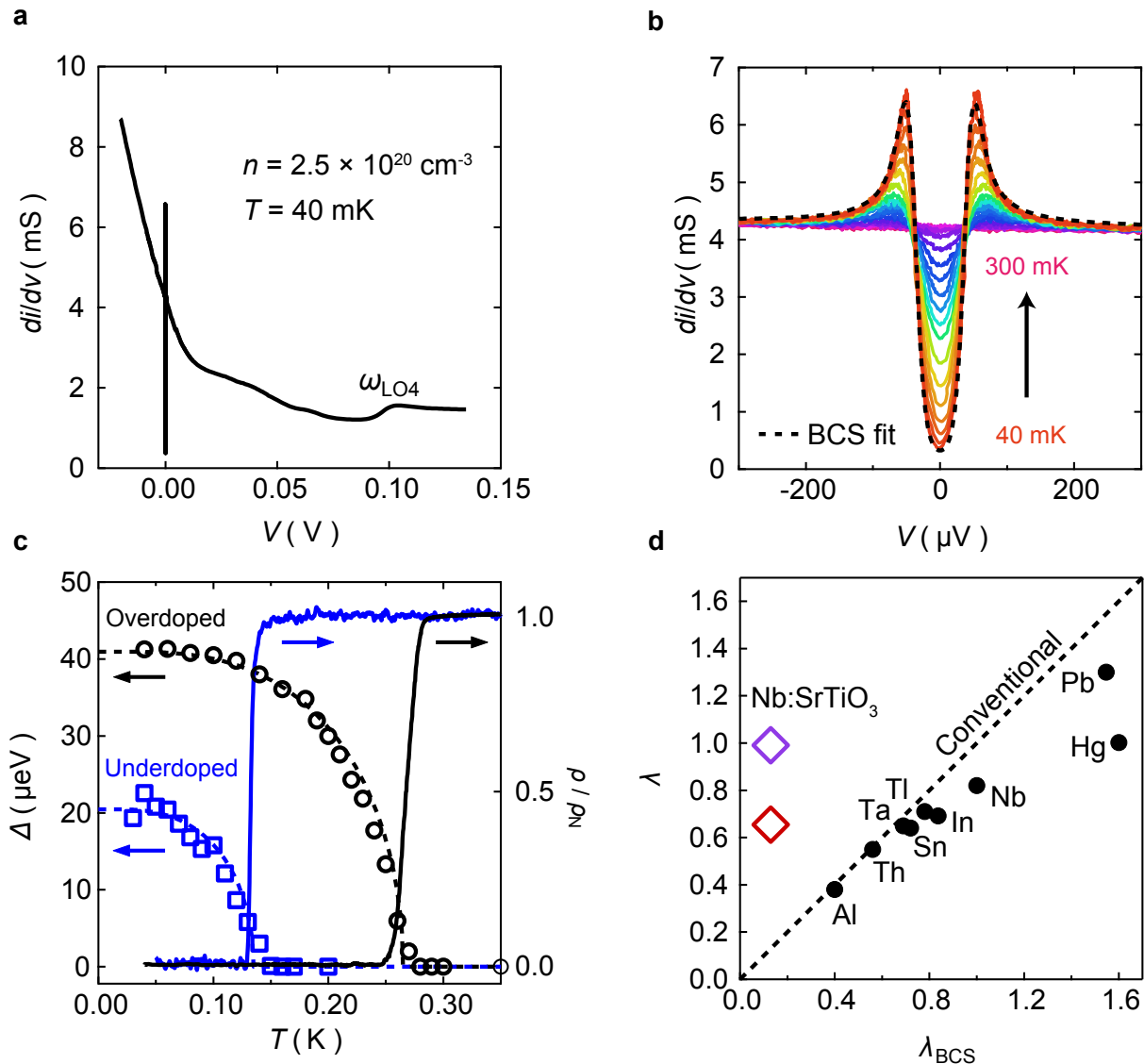


Figure 4.